Capillary Stem Cells Enhance Vascular Barrier Function Revealed by the In Vitro Microvessel Model

Hedele Zeng, Takanori Sano, Jean Cacheux, Aurélien Bancaud, Jun-Ichi Kawabe, Yukiko T Matsunaga

ORIGINAL ARTICLE

Capillary Stem Cells Enhance Vascular Barrier Function Revealed by the *In Vitro* Microvessel Model

Hedele ZENG[1,2], Takanori SANO[1], Jean CACHEUX[1,3], Aurélien BANCAUD[1,3], Jun-ichi KAWABE[4], and Yukiko T. MATSUNAGA[1,2,3]

[1] *Institute of Industrial Science, The University of Tokyo, Tokyo, Japan*
[2] *Department of Bioengineering, School of Engineering, The University of Tokyo, Tokyo, Japan*
[3] *LIMMS, CNRS-IIS UMI 2820, The University of Tokyo, Tokyo, Japan*
[4] *Department of Biochemistry, Asahikawa Medical University, Asahikawa, Japan*

Synopsis
Mesenchymal stem cells (MSCs) have received attention in the field of regenerative medicine due to their broad-ranging differentiation potential and strong secretory function. Although some studies have shown that MSC transplantation rescues blood flow, its contribution to the repair of microvasculature at the cell-to-tissue level is still obscure. To understand the mechanism of the MSC therapy for ischemic diseases, we developed a three-dimensional (3D) microvessel model cocultured with EphA7$^+$ MSC-like capillary derived pericytes, termed capillary stem cells (CapSCs). It was shown that cocultured CapSCs within the collagen gel matrix tend to accumulate around the microvessel, accompanied with junctional expression VE-cadherin on the endothelial layer. In addition, the barrier function assay showed CapSCs strengthen the endothelial barrier.

Key words: *Mesenchymal stem cells (MSCs), capillary stem cells (CapSCs), capillary endothelial barrier, permeability assay, in vitro 3D model*

Introduction

Ischemia is characterized by a local insufficient blood supply typically resulting from by abnormal vascular conditions such as plaque attachment and blood clots [1]. Recently, a study reported that 126 million people are suffered from ischemic heart disease (IHD) and 9 million people died from IHD in 2017 [2]. Stem cell-based regenerative therapy, which can stabilize the existing microvessel, promote the angiogenetic process, repair damaged vasculatures, and improve the whole microcirculation, has been considered as a promising candidate in ischemia treatment [3].

Pericyte (PC) plays a pivotal role in vascular barrier regulation, and ischemia-induced PC loss has been found to result in disordered inflammatory response and microcirculation defects [4]. Mesenchymal stem cells (MSCs) are a group of multipotent cells endowed with mesodermal phenotypes and it is generally believed that the majority of MSCs can be derived from PCs [5]. Nowadays, MSCs have received worldwide attention in chronic hepatitis [6], arthritis disease [7], and tumor treatment [8], due to their broad-ranging differentiation potential and strong secretory function. For vascular function repair, previous studies have shown that MSCs are capable of preserving the vessel barrier function by (i) attenuating matrix metallo-

proteinase and pro-inflammatory factors upregulation of endothelial cells (EC), (ii) reinforcing EC-PC interaction through growth factor secretion, and (iii) working as a substitute in case of loss of PCs [9]. We also have recently shown that EphA7+ MSC-like capillary derived pericytes, termed capillary stem cells (CapSCs) were more effective than conventional PC transplantation regarding neovessel formation and blood perfusion recovery from hind limb ischemia [10].

Nevertheless, the species difference in animal models made it hard to infer human biological responses and therefore limited the therapeutic potential of the transplantation treatment while clinical trials always have strict ethical requirements. Additionally, the organ-level treatment efficiency evaluation can elongate the trial time and increase economic cost [11]. The sophisticated 3D models, microphysiological systems (MPS), have received widespread attention as platforms for drug screening and biological investigation. This new type of tool recapitulates *in vivo* structures and functions that are difficult to emulate with conventional 2D cultures, while requiring less costs and time compared with traditional animal experiments. Besides, MPSs provide less interference caused by individual differences, which is beneficial for biological investigations [12].

To evaluate the potential of CapSCs to maintain vascular barrier integrity following ischemia treatment, we constructed a 3D microvessel model cocultured with CapSCs. In this culture system, ECs were seeded and cultured in hollow cylindrical tubes made from collagen gel to form an in vivo-like vessel structure. This design makes it possible to see how CapSCs affect angiogenesis, vascular morphogenesis, and enhance vascular functions at the tissue level from a quantitative perspective.

Material and Method

1. Cell culture

1) HUVECs

Human umbilical vein endothelial cells (HUVECs) and Endothelial Cell Growth Medium-2 BulletKit (EGM-2) were purchased from Lonza (Basel, Switzerland). HUVECs between passages 4 and 7 were used in this study.

2) CapSCs

Multipotent pericytes with EPH receptor A7 (EphA7, NCBI-GeneID: 2045) expression, termed capillary stem cells (CapSCs) were isolated from the capillary-rich fraction of green fluorescent protein (GFP) gene-expressing mice (C57BL/6J background, male, 12-16 weeks of age) subcutaneous adipose tissues, by using anti-EphA7 antibody (LSBio, LS-C164376, Seattle, WA, USA). The isolation method has been described previously [10]. The animal procedures were approved by the Animal Care and Use Committee of Asahikawa Medical University.

Gibco™ Dulbecco's Modified Eagle Medium (DMEM) (low glucose, with GlutaMAX™ supplement and pyruvate) was purchased from ThermoFisher Scientific (Waltham, MA, USA). As CapSC culture medium, DMEM medium was mixed with 4% fetal bovine serum (FBS; Biosera, Nuaille, France), insulin-transferrin- selenium-sodium pyruvate (ITS-A) (100×) (Gibco, Thermo Fisher Scientific, Waltham, MA, USA), penicillin -streptomycin (FUJIFILM Wako, Osaka, Japan), 0.05% bovine serum albumin (BSA) (Sigma-Aldrich, St. Louis, MO, USA), 20 ng/mL recombinant murine epidermal growth factor (EGF), and 20 ng/mL recombinant murine fibroblast growth factor (FGF)-basic (PeproTech, Cranbury, NJ, USA). CapSCs were maintained in the above media and passages between 10 and 12 were used in this study.

2. Three-dimensional CapSC-EC coculture model

Cellmatrix® Type I-A (acid-extracted collagen I isolated from porcine tendons, 3 mg/mL, pH 3) was purchased from Nitta Gelatin Inc. (Osaka, Japan). 10×collagen buffer was prepared by dissolving $NaHCO_3$ 262 mM (Kanto Chemical, Tokyo, Japan), NaOH 0.05 N (Kanto Chemical), and HEPES 20 mM (Sigma-Aldrich, St. Louis, MO, USA) into sterile water. Acupuncture needles (J type, No.02, 200-μm diameter and 30-mm length) were purchased from Seirin Co. Ltd. (Shizuoka, Japan). 10 × phosphate-buffered saline (PBS) was purchased from FUJIFILM Wako Pure Chemical Industries Ltd. (Osaka, Japan). Dextran from Leuconostoc spp., (Mr 450,000-650,000) and Hanks's balanced salt solution (HBSS) were purchased from Sigma-Aldrich (St. Louis, MO, USA). Rhodamine-conjugated Ulex europaeus Agglutinin I lectin (UEA-I) was purchased from Vector Laboratories (Burlingame, CA, USA). Water was collected from Milli-Q system (Merck KGaA,

Darmstadt, Germany).

Previously described polydimethylsiloxane (PDMS)-based chips were used to fabricate microvessel models [13, 14]. For the CapSC-EC coculture model, the cell concentration of CapSC suspension was first counted by using the hemacytometer and the necessary suspension volume that contains 2×10^4 CapSCs was calculated and collected in a separate tube in advance. After centrifugation and supernatant liquid removal, CapSCs were mixed with 40 μL of 2.4 mg/mL Cellmatrix solution with collagen buffer and HBSS (8:1:1 volume ratio) and poured in the chip chamber. Similarly, EC monoculture chips were fabricated with 40 μL pure 2.4 mg/mL Cellmatrix solution. Monoculture group and coculture group were prepared together. An acupuncture needle coated with 1% BSA in PBS solution was inserted into the chip from the side before gel solidification. The needle was removed after one day, and 4 μL of HUVECs suspension in 1×10^7 cells/mL concentration was added into the side wells. 1 mL warmed EGM-2 medium was added to each chip finally. The same amount of EGM-2 medium was changed once a day.

3. Immunofluorescence

CapSC-EC coculture and EC monoculture chips were fixed with 4% PFA solution after a 5-day culture, washed with PBS, and blocked with 1% BSA in PBS solution within a 4°C fridge overnight. Then 1:200 ratio diluted VE-Cadherin (D87F2) XP® Rabbit mAb antibody solution (Cell Signaling, Danvers, MA, USA) was added to the chips. After being stored in a 4°C fridge overnight and after completion of the 1st antibody washout, 1:800 ratio diluted Goat anti-Rabbit IgG (H+L) Cross-Adsorbed antibody (Alexa Fluor® 555) and 1:1,000 ratio diluted Hoechst 33342 (Thermo Fisher Scientific, Waltham, MA, USA) were mixed and added to chips. The chips were wrapped with aluminum foil and placed under 25°C for three hours and then washed with PBS.

4. Microscopy

Morphological observations were performed by a confocal laser scanning microscope (CLSM; LSM 700, Carl Zeiss, Oberkochen, Germany) using a 20× objective lens (Plan-Apochromat 20×/ 0.8 and LD Plan-NeoFluar 20×/0.4 Korr M27) in z-stack mode (126 slices, 2 μm interval). A 4×2 image z-stack scanning tile was recorded and stitched for each acquisition. EC-EC junction observations were done with a 40× objective lens (LD C-Apochromat 40×/ 1.1 W Korr M27). Images were processed by the ZEN 2 blue edition software (version 2.0.0.0, Carl Zeiss) and FIJI to extract pixel intensity and to create z-stack maximum intensity projections (MIP).

5. Permeability assay

To evaluate the barrier function of the microvessel wall, 10 μg of 4kDa fluorescein isothiocyanate-dextran (FITC-dextran, Sigma-Aldrich, St. Louis, MO, USA) was diluted in 1 mL PBS solution, and 30 μL of this solution was injected in the vessel. Time-lapse CLSM imaging was then performed using a 10×objective lens (N-Apochromat 10×/0.25 M27). The fluorescence intensity of the microvessel area, the collagen gel area, and the microvessel diameter were extracted and calculated by a dedicated FIJI macro.

Here, we assume the EC layer around the central lumen as a porous sheet. The fluorescent tracers freely diffuse through the holes and cannot pass the cell soma. Since the free diffusion process follows Fick's law and the flux can be calculated through the temporal change of integration of fluorescence intensity, the porosity of the EC tissue can be calculated. The porosity (Equation-1) is defined by the area of void space over the total surface. This quantitative overall porosity measurement has been comprehensively described in the previously published study [15].

$$\varphi = \frac{Area_{pore}}{Area_{whole}} = n\pi r_p^2 \qquad (1)$$

where n is the density of pores per unit of surface and r_p is the average radius of the pores.

The flux of fluorescent dextran molecules $J(t)$ across the barrier is equal to the temporal variation of the number $N_{out}(t)$ outside of the vessel barrier. We consider a diffusion process, implying that the flux $J(t)$ is proportional to the difference between the internal and external concentrations C_{in}, and C_{out} (*i.e.*, we assume the Fick's law to be relevant).

The proportionality factor is the diffusive permeability $\mathcal{L}_D$ described in previous research (Equation-2) [16, 17].

$$J(t) = \frac{dN_{out}(t)}{dt} = 2\pi r_0 \mathcal{L}_D\big(C_{in}(t) - C_{out}(t)\big) \qquad (2)$$

We can therefore express the diffusive permeability as a function of experimental readouts in (Equation-3):

$$\mathcal{L}_D = \frac{dN_{out}/dt}{2\pi r_0(C_{in} - C_{out})} \quad (3)$$

The $\mathcal{L}_D$ is proportional to the porosity φ, the tissue thickness δ, and the diffusion coefficient in the pore D_p in a Fick's law governed diffusion:

$$\mathcal{L}_D = \frac{\varphi}{\delta} D_p \quad (4)$$

Note that we disregard the consequence of the hindrance associated to the excess of friction for a probe traversing a narrow pore and assume D_p equal to marker diffusion coefficient D_o [16, 17]. Accordingly, we can calculate the porosity φ by integrating Equation-3 and -4.

Here, the diffusion coefficient D_0 of the 4-kDa FITC dextran dye was 244 ± 25 $\mu m^2/s$, and we empirically set the thickness δ 3.2 μm.

6. Statistical analysis

Data are presented as the mean ± standard deviation. Statistical significance between groups was determined using the unpaired Student's t-test. All data were analyzed using Microsoft 365 Excel (Microsoft, Redmond, WA, USA), FIJI, or MATLAB (MathWorks, Natick, MA, USA).

Results

A 3D microvessel was fabricated within a collagen gel seeded with CapSCs (Fig. 1A). Z-stack maximum intensity projection (MIP) images show the temporal morphological change of the coculture microvessel and the migration of the surrounding CapSCs (Fig. 1B). Although the density of CapSCs within the collagen gel area was relatively stable during 5 days of culture, CapSCs in contact with the microvessel surface increased over time. Monoculture and coculture chips kept their global vessel-like appearances (Fig. 1C).

Nevertheless, many small sprouts and dissociated single ECs in the collagen gel were observed in the monoculture (upper panel of Fig. 1C). On the contrary, only few but morphologically mature sprouts can be seen in the coculture chip (middle panel of Fig. 1C). The average sprout number of monoculture chips was twice that of coculture chips after 5-day culture: 20.67 ± 2.05 in monoculture and 10.3 ± 3.09 in coculture, respectively. Enlarged images indicate an attachment of CapSCs to the sprout root and tip area (lower panel of Fig. 1C).

To investigate the barrier function of the endothelium on the microvessels, we used FITC-labelled dextran (4 kDa), measuring its passive diffusion across the microvessel wall from inside of luminal structure to outside. The confocal microscopies showed that there were few leakages along the coculture chip, compared with a large leakage on the monoculture chip (Fig. 2A, left). The temporal change of the central line fluorescence intensity changes supported this conclusion (Fig. 2A, right). Quantitative analysis showed that the existence of CapSC decreased the mean vessel porosity (0.062% ± 0.04%) to nearly one-ninth of that of the monoculture (0.58% ± 0.31%) (Fig. 2B). To provide biological evidence for this result, EC adherens junctions have been characterized by immunostaining and results show that cocultured microvessels had a higher VE-cadherin expression between EC-to-EC than the monoculture ones (Fig. 2C).

Discussion

By using the in vitro microvessel model cocultured with CapSCs, we found that the time-dependent CapSC localization on the surrounding microvessel surface, which is similar to the migration of pericytes *in vivo* mentioned in other studies [18, 19]. These results suggest that the CapSC we used in this experiment may be efficient to support the microvessel through both direct structural contact and indirect secretion, which is in accordance with the results in our previous research [20]. The comparison between the monoculture and coculture microvessel demonstrated that the presence of CapSCs may regulate the EC migration and contribute to the formation of morphologically mature sprouts (Fig. 1C). In this study, we did not evaluate whether if CapSCs maintained their stemness or differentiation into ECs or PCs. However, in our previous study, gene expression of EC markers such as von Willebrand Factor (vWF) and platelet endothelial cell adhesion molecule 1 (PECAM-1) was significantly increased when CapSCs were grown and formed self-assembled tube-like structure within a Matrigel in the presence of VEGF [10].

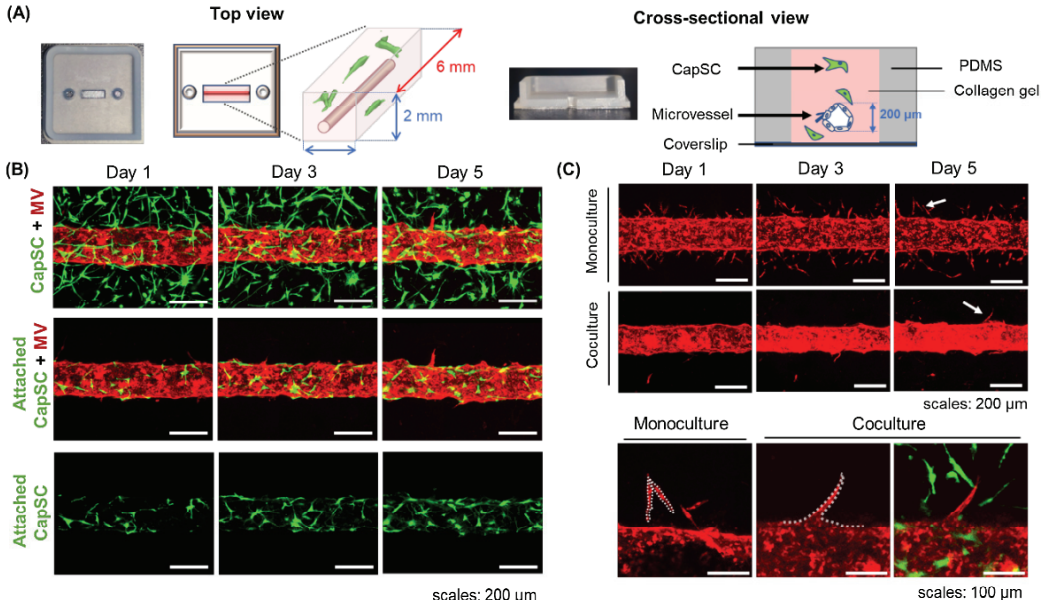

Figure 1 Fabrication of microvessel model cocultured with CapSCs. (A) Photographs and schematic illustrations of coculture microvessel (MV) model. (B) Time-dependent CLSM z-stack MIP images of the coculture microvessel and the area of microvessel attached with CapSCs. (C) Time-dependent CLSM z-stack MIP images of the monoculture and the coculture microvessel. Representative angiogenic sprouts area on Day 5 indicated by white arrows were enlarged below and the boundaries of the sprouts were highlighted by white dotted lines. HUVECs forming microvessels were stained with UEA-I (red) and GFP-expressing CapSCs (green) were encapsulated in the collagen gel (B and C).

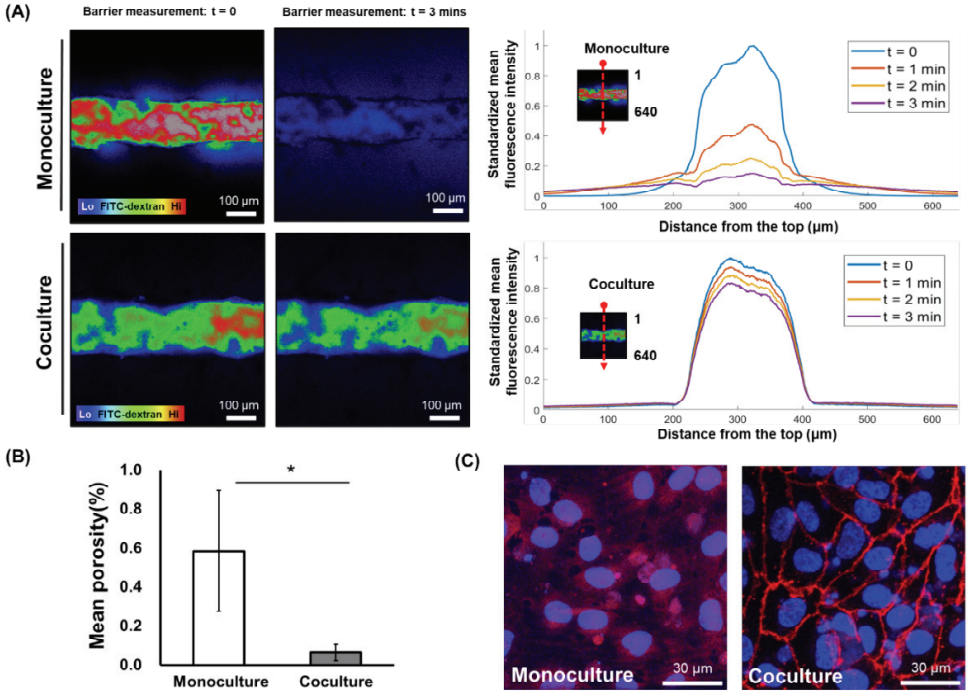

Figure 2 Evaluation of barrier function of endothelium in microvessel model. (A) CLSM images of FITC-dextran (4 kDa) leaking from 5-day cultured microvessels into the collagen gel (color-scaled image) at each time point: t = 0 or 3 min, respectively (left), and the temporal change of the standardized mean fluorescence intensity along the image central line during the barrier function assay (right). (B) Quantification of the mean equivalent vascular tissue porosity in passive diffusion. The leakages for four microvessels per experimental condition were quantified. The data are presented as the mean ± s.d.. Significant differences between monoculture and coculture were analyzed by two-tailed unpaired Student's t-test. *$p < 0.05$, $n = 4$. (C) Representative CLSM MIP images of immunostained adhesive junction (VE-cadherin) of endothelium in microvessel models colored in red and nuclei stained with Hoechst 33342 colored in blue on Day 5.

Using FITC-dextran, we visualized the leakage of the microvessel and quantified the vascular barrier function. We found that a fast decrease of fluorescence intensity within the monocultured microvessel lumen area, which may be corresponding to the disconnected sprouts and "escaped" single EC demonstrated in Fig. 1C. VE-cadherin is a component of endothelial cell-to-cell adherens junctions, and it has a key role in the maintenance of vascular integrity such as permeability control and vascular development. Fig. 2C showed that there was no strong VE-cadherin signal between ECs in the monoculture sample and some holes were observed, while the strong VE-cadherin signal was present around the EC boundary in the coculture sample, which indicated that the CapSCs in coculture chips greatly increased the VE-cadherin expression of ECs. The maintenance of strong adhesion between ECs also explained that the cells merely escaped in the matrix in immature sprouts in the monoculture, whereas few mature sprouts appeared in the coculture microvessels.

Conclusion

In conclusion, this study proposed a 3D microvessel model cocultured with CapSCs that could recapitulate the physiological barrier function and angiogenesis process during a 5-day continuous culture. The coculture chip showed a different angiogenesis dynamic and barrier function from the EC monoculture chip. The microvessel in the coculture chip had smaller morphological changes, fewer sprouts, and better barrier function than the monoculture microvessel. Besides, the sprouts in the coculture chip also showed a higher morphological maturity. For barrier function, the existence of CapSC has been found to greatly increase the VE-cadherin expression among ECs. Quantitative permeability assay revealed that these morphological and molecular changes dramatically enhanced vascular barrier function, demonstrating the efficacy of CapSCs in the treatment of vascular disease.

Acknowledgments

We would like to thank Mr. Daniel Martin Alcaide (The University of Tokyo) and Mr. Ian Schumacher (ETH Zurich) for their valuable comments. H.Z. acknowledges the financial support of Otsuka Toshimi Scholarship Foundation, and the fellowship from JST SPRING (Grant Number JPMJSP2108).

References

1) Yong KW, Choi J R, Mohammadi M, Mitha AP, Sanati-Nezhad A, Sen A. Mesenchymal stem cell therapy for ischemic tissues. Stem Cells Int 2018; 2018: 1-11.
2) Khan MA, Hashim MJ, Mustafa H, Baniyas MY, Al SS, Alkatheeri R, Alblooshi F, Almatrooshi M, Alzaabi M, Al D R, Lootah S. Global epidemiology of ischemic heart disease: Results from the global burden of disease study. Cureus 2020; 12: e9349. DOI: 10.7759/cureus.9349
3) Hoang D M, Pham P T, Bach T Q, Ngo A T L, Nguyen Q T, Phan T T K, Nguyen G H, Le P T T, Hoang V T, Forsyth N R, Heke M, Nguyen L T. Stem cell-based therapy for human diseases. Signal Transduction and Targeted Therapy 2022; 7: 272. DOI: 10.1038/s41392-022-01134-4
4) Zhou S, Guo Z, Zhang D, Qu Y, Jin H. The Role of Pericytes in Ischemic Stroke: Fom cellular functions to therapeutic targets. Front Mol Neurosci 2022; 15: 866700. DOI: 10.3389/fnmol.2022.866700
5) Caplan A I. New MSC: MSCs as pericytes are Sentinels and gatekeepers. J Orthop Res 2017; 35: 1151-1159.
6) Fang X, Liu L, Dong J, Zhang J, Song H, Song Y, Huang Y, Cui X, Lin J, Chen C, Liu B, Chen Z, Pan J, Chen X. A study about immunomodulatory effect and efficacy and prognosis of human umbilical cord mesenchymal stem cells in patients with chronic hepatitis B-induced decompensated liver cirrhosis. J Gastroen Hepatol 2018; 33: 774-780.
7) Jevotovsky DS, Alfonso A R, Einhorn T A, Chiu E S. Osteoarthritis and stem cell therapy in humans: a systematic review. Osteoarthr Cartilage 2018; 26: 711-729.
8) Liang W, Chen X, Zhang S, Fang J, Chen M, Xu Y, Chen X. Mesenchymal stem cells as a double-edged sword in tumor growth: focusing on MSC-derived cytokines. Cell Mol Biol Lett 2021; 26: 3. DOI: 10.1186/s11658-020-00246-5
9) Do P T, Wu C, Chiang Y, Hu C, Chen K. Mesenchymal stem/stromal cell therapy in blood–brain barrier preservation following ischemia: Molecular mechanisms and prospects. Int J Mol Sci 2021; 22: 10045. DOI: 10.3390/ijms221810045
10) Yoshida Y, Kabara M, Kano K, Horiuchi K, Hayasaka T, Tomita Y, Takehara N, Minoshima A, Aonuma T, Maruyama K, Nakagawa N, Azuma N, Hasebe N, Kawabe J. Capillary-resident EphA7+ pericytes are multipotent cells with anti-ischemic effects through capillary formation. Stem Cell Transl Med 2020; 9: 120-130.
11) Gupta PK, Krishna M, Chullikana A, Desai S, Murugesan R, Dutta S, Sarkar U, Raju R, Dhar

A, Parakh R, Jeyaseelan L, Viswanathan P, Vellotare P K, Seetharam R N, Thej C, Rengasamy M, Balasubramanian S, Majumdar A S. Administration of adult human bone marrow-derived, cultured, pooled, allogeneic mesenchymal stromal cells in critical limb ischemia due to buerger's disease: Phase II study report suggests clinical efficacy. Stem Cell Transl Med 2017; 6: 689-699.
12) Benam KH, Gilchrist S, Kleensang A, Satz AB, Willett C, Zhang Q. Exploring new technologies in biomedical research. Drug Discov Today 2019; 24: 1242-1247.
13) Pauty J, Usuba R, Cheng I G, Hespel L, Takahashi H, Kato K, Kobayashi M, Nakajima H, Lee E, Yger F, Soncin F, Matsunaga YT. A vascular endothelial growth factor-dependent sprouting angiogenesis assay based on an in vitro human blood vessel model for the study of anti-angiogenic drugs. Ebiomedicine 2018; 27: 225-236.
14) Pauty J, Nakano S, Usuba R, Nakajima T, Johmura Y, Omori S, Sakamoto N, Kikuchi A, Nakanishi M, Matsunaga YT. A 3D tissue model-on-a-chip for studying the effects of human senescent fibroblasts on blood vessels. Biomater Sci-Uk. 2021; 9: 199-211.
15) Cacheux J, Bancaud A, Alcaide D, Suehiro J, Akimoto Y, Sakurai H, Matsunaga YT. Endothelial tissue remodeling induced by intraluminal pressure enhances paracellular solute transport. iScience. 2023; 26: 107141. DOI: 10.1016/j.isci.2023.107141
16) Michel CC, Curry FE. Microvascular permeability. Physiol Rev 1999; 79: 703-761.
17) Mari Hämäläinen K, Kontturi K, Auriola S, Lasse Murtomäki, Urtti A. Estimation of pore size and pore density of biomembranes from permeability measurements of polyethylene glycols using an effusion-like approach. J Control Release 1997; 49: 97-104.
18) Stratman AN, Malotte KM, Mahan RD, Davis MJ, Davis GE. Pericyte recruitment during vasculogenic tube assembly stimulates endothelial basement membrane matrix formation. Blood 2009; 114: 5091-5101.
19) Wang Y, Jin Y, Laviña B, Jakobsson L. Characterization of multi-cellular dynamics of angiogenesis and vascular remodelling by intravital imaging of the wounded mouse cornea. Sci Rep-Uk 2018; 8: 10672. DOI: 10.1038/s41598-018-28770-7
20) Sano T, Nakajima T, Senda K A, Nakano S, Yamato M, Ikeda Y, Zeng H, Kawabe J, Matsunaga YT. Image-based crosstalk analysis of cell–cell interactions during sprouting angiogenesis using blood-vessel-on-a-chip. Stem Cell Res Ther 2022; 13: 532. DOI: 10.1186/s13287-022-03223-1

(Received: December 15, 2023/
Accepted: December 23, 2023)

Corresponding author:
Prof. Yukiko T. Matsunaga, Ph.D.
Institute of Industrial Science,
The University of Tokyo 4-6-1 Komaba,
Meguro-ku, Tokyo
153-8505, Japan
Tel.: +81-3-5452–6470
Fax : +81-3-5452-6471
E-mail: mat@iis.u-tokyo.ac.jp